On the Abundance and Common Properties of Continental, Organized Shallow (Green) Clouds

Tom Dror, Ilan Koren, Orit Altaratz, and Reuven H. Heiblum

***Abstract*— Warm convective clouds play a significant role in the earth's energy and water budgets. However, they still pose a challenge in climate research as their feedback to predicted thermodynamic changes is highly uncertain and considered critical to the overall climate system's response. The focus of this study is continental, organized shallow convective clouds that, although they are spread globally and form in a variety of environments, seem to have common properties. One of these properties seems to be their preferred formation over vegetated areas, thus referred hereafter as green Cu. In this article, we present new observations of emerging universality and explore them using a method that combines fine- and coarse-resolution remote-sensing data sets. First, we use Moderate Resolution Imaging Spectroradiometer (MODIS) true-color images to visually classify cloud fields into different classes and identify green Cu fields. We show that the level and type of organization and the properties of these fields (e.g., cloud size distribution and cloud fraction) are similar throughout the world, regardless of their location. Second, we match the corresponding MODIS level-3 cloud properties to the identified cloud classes, and based on this data sets statistics, we develop a detection method for green Cu along ten years of measurements (2003–2012). We examine the geographical distribution and seasonality of this class and show that these fields are highly abundant over many continental areas and indeed mostly in the vicinity of vegetated regions.**

***Index Terms*— Cloud classification, cloud remote sensing, continental clouds, fair weather cumulus, Moderate Resolution Imaging Spectroradiometer (MODIS), satellite applications, shallow cumulus.**

I. Introduction

CLOUDS play a key role in the earth's energy balance and water cycle [1]. However, despite extensive research, clouds still prevent confident predictions of climate [2]–[4]. More specifically, shallow warm cumulus clouds (shallow Cu) pose one of the toughest challenges in climate research since they constitute a major source of uncertainty in tropical cloud feedback in climate models [5], [6], and their properties often cannot be obtained from space [7]. Those clouds, often called 'fair weather cumulus' (FWC; which is a traditional morphological classification, equivalent to cumulus humilis or mediocris, World Meteorological Organization (WMO), 1969), increase the planetary albedo and decrease the shortwave radiation at the surface while having little influence on the longwave radiation budget [8]–[10]. Shallow Cu affect the transport of mass, momentum, moisture, and pollutants from the boundary layer to the free troposphere [11]. Thus, an accurate representation of their processes and properties in atmospheric models is essential for adequately simulating the fluxes in the current and in predicted changing climates. Moreover, shallow Cu plays an important role in preconditioning the atmosphere for deep clouds development [12]. A better understanding of the warm processes controlling the development of shallow Cu is important for an understanding of deep convective clouds [13] because the former essentially serve as the boundary conditions for the development of deep mixed-phase clouds. Nevertheless, being on the order of $\sim$1 km in size [11], [14], shallow Cu are a subgrid-scale phenomenon in most of the atmospheric models and therefore are not explicitly resolved, but are represented via parameterizations [9]. Recent studies have shown that those parameterizations are one of the key problems in both numerical weather prediction and climate models simulations [5], [15], [16]. As a result, general circulation models (GCMs) suffer from errors in the location, timing, and extent of both shallow and deep convective clouds [17].

Compared to marine shallow Cu (i.e., the well-known trade cumulus), continental shallow Cu have received less scientific attention [18]. The forcing behind continental shallow Cu formation is both stronger and time variant compared with the relatively statistically steady convection over the ocean [12], [13], [19]. This variability makes these clouds more difficult to study.

Over land, shallow Cu usually form during the warm (or dry) season [20]. Since continental shallow Cu are closely linked to thermal convection, their properties are tightly coupled with the diurnal cycle of surface fluxes, boundary layer stability, and relative humidity. They usually form around mid or late morning when the boundary layer depth (controlled by the interplay between the surface fluxes, the static stability of the atmosphere above the boundary layer, and large-scale subsidence or lifting) grows above the altitude of the lifting condensation level (LCL; quantifying the amount of moisture in the lower part of the boundary layer) [9] and dissipate after sunset [11], [21], [22] if they do not transition to deep convective clouds in the late afternoon (a case which requires supportive meteorology [23], [24]).

Manuscript received March 29, 2020; revised August 3, 2020; accepted September 6, 2020. Date of publication September 25, 2020; date of current version May 21, 2021. This work was supported by the European Research Council (ERC) through the European Union's Horizon 2020 Research and Innovation Program under Grant 810370. *(Corresponding author: Ilan Koren.)*

The authors are with the Department of Earth and Planetary Science, Weizmann Institute of Sciences, Rehovot 7610001, Israel (e-mail: tom.drorschwartz@weizmann.ac.il; ilan.koren@weizmann.ac.il; orit.altaratz@weizmann.ac.il; reuven.heiblum@weizmann.ac.il).

Color versions of one or more of the figures in this article are available online at https://ieeexplore.ieee.org.

Digital Object Identifier 10.1109/TGRS.2020.3023085

Previous work has examined continental shallow Cu in different regions throughout the world, focusing mainly on the Southern Great Plains (SGP) [9], [11], [12], [14], [25], [26] and the Amazon basin [27]–[29]. Specifically, toward improving the representation of shallow Cu in GCMs and numerical weather prediction models, factors such as their cloud size distribution (CSD) and diurnal cycle, are being extensively studied. A number of studies have examined the size distributions of shallow Cu over land. Some of them have reported an exponential CSD shape [9], [30]–[32], and others a power-law behavior [33]–[37]. However, none of these studies performed a systematic analysis of the clouds on a global scale. Here, we examine the properties of shallow continental Cu. Our analysis reveals that these clouds, observed from low- to mid- and high-latitudes in a variety of climatic regions, share universal behavior and appearance. Namely, in many cases, continental shallow convective clouds exhibit similar properties, such as cloud cover, CSD, organization pattern, and preferred formation in the vicinity of vegetated area, thus referred to hereafter as green Cu. This can be clearly seen for the three different regions shown in Fig. 1(a)–(c). We explore the universal properties and prevalence of green Cu fields. Using a combination of coarse- and high-resolution remote-sensing data, we globally identify these cloud fields, examine the similarities between them across the world's continents, and quantify their abundance, with a special focus on cloud fields that form over and near forests and vegetated areas.

II. Methodology

A. Regions of Interest

To study the abundance and properties of green Cu, we chose three vast ($14^\circ \times 14^\circ$) regions of interest (ROIs) that are known to exhibit shallow convection during the northern hemisphere (NH) summer (dry season in the tropics; June–July–August [JJA]). The first ROI is located in the Amazon basin and spans the area between $3^\circ S - 17^\circ S$ and $63^\circ W - 49^\circ W$, the second is located in the central USA, spanning the area between $30^\circ N - 44^\circ N$ and $96^\circ W - 82^\circ W$, and the third ROI is located in Eastern Europe and spans the area between $46^\circ N - 60^\circ N$ and $27^\circ E - 41^\circ E$. Fig. 1(a)–(c) shows a $1^\circ \times 1^\circ$ area from each region, and the locations of the ROIs superimposed on a global topography map are shown in Fig. 1(d) (see black boxes). The three examined ROIs exhibit different climates and different large-scale circulations. The Amazon, USA, and Eastern Europe are categorized by the Köppen climate classification as tropical savanna climate, humid subtropical/continental climate, and humid continental mild/hot summer, respectively [38]. During the NH summer, as the pole-to-equator temperature gradient is reduced, the Intertropical Convergence Zone (ITCZ) reaches its northward displacement ($\sim 10^\circ N$) and the Amazon region is dominated by the South Atlantic Subtropical High [39]. At the same time, the extratropical storm track over midlatitudes weakens and migrates poleward [40], resulting in periods of anticyclonic conditions [41], [42] in the USA and Eastern Europe ROIs. These large-scale patterns can drive periods during the NH summer, for which there is subsidence at middle atmosphere accompanied by a humid boundary layer and moderate surface winds that support the formation of green Cu fields in the three ROIs [43]. As is evident from Fig. 1(d), the three ROIs, Amazon, USA, and Eastern Europe, have low-altitude topography (271.6 ± 152.2, 208.7 ± 123.9, and 142.6 ± 54.5 m, respectively); moreover, they all share moderate gradients in the topography, with mean slopes (θ) of $=0.0378^\circ$, 0.0351°, and 0.0212°, respectively.

B. Remote-Sensing Data

We used measurements from the Moderate Resolution Imaging Spectroradiometer (MODIS) [7], [44], [45] onboard the Aqua satellite for the years 2003–2012. Aqua's orbit architecture is timed to cross the equator from south to north (ascending mode) at approximately 13:30 local solar time. At this time, the surface fluxes are maximal, which enables Aqua to capture the cloud fields around their daily peak of development in terms of many of the clouds' properties (e.g., cloud fraction [CF], cloud top height [CTH], cloud depth, and liquid water path) [11]–[13].

For the first stage, visual classification of the cloud fields (and their morphological analysis), we used high-resolution (500 m) true-color images, while cloud properties (CF and CTH) used for the second stage of globally identifying green Cu fields, were derived from MODIS daily level-3 data (L3; with a spatial resolution of $1^\circ \times 1^\circ$). Each $14^\circ \times 14^\circ$ ROI was divided into smaller $1^\circ \times 1^\circ$ subsets, each composed of 228×228 pixels (representing the scale of the cloud field, hereafter cloud fields). This was done while excluding the regions located up to 300 km from the granule edges, to avoid averaging cloud properties over two MODIS overpasses, and pixel distortion issues (i.e., "bow-tie-effect" [46]). The green Cu fields' data set, obtained by the visual classification, is comprised of a total number of 58, 47, and 43 MODIS overpasses (i.e., days) for the Amazon, USA, and Eastern Europe ROIs, respectively. The cloud fields were centered around half of a degree to match the MODIS L3 grid.

Land cover data were taken from the European Space Agency (ESA) Climate Change Initiative Land Cover (CCI-LC) project [47]. Here, we used the 2007 CCI-LC map. We chose 2007 as a representative year for the time span of the analysis (2003–2012) because comparison of the land cover maps for 2003 and 2012 showed only minor modifications, which were explained by the coarse resolution at which we inspected the changes ($1^\circ \times 1^\circ$). The map depicts the geographical distribution of global land cover at a resolution of 300 m. We aggregated the map into $1^\circ \times 1^\circ$ resolution using the CCI-LC user tool to match it to the cloud fields and MODIS L3 resolution.

C. Morphological Analysis

We used high-resolution (500 m) satellite data in the visible for calculating morphological properties of $1^\circ \times 1^\circ$ cloud fields (228×228 pixels). First, we constructed a cloud mask based on the one developed by [29]. While there are many cloud detection algorithms (see [48]–[50] and others), here, we used the one based on [29] since it was constructed

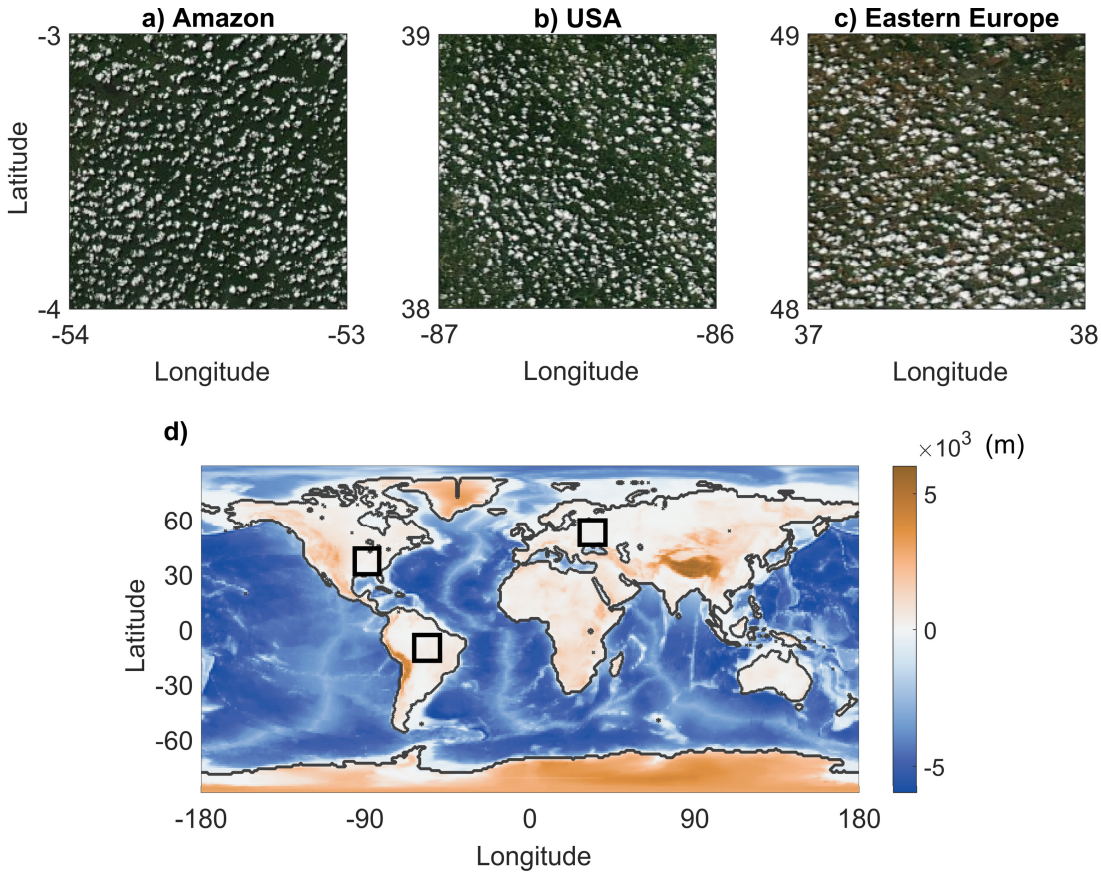

Fig. 1. Example of a 1° × 1° green Cu field over (a) Amazon basin, (b) central USA, and (c) Eastern Europe. (d) Global topography (height above mean sea level) map. Black boxes represent the three different ROIs.

specifically for investigating continental shallow clouds over the Amazon, using MODIS RGB channels. A threshold of >0.39 was applied to the reflectance of the RGB channels (bands 1, 3, and 4, respectively). Bright pixels that are not clouds (e.g., deforested areas and bright roads) are not white, and they therefore have spectral dependence in the visible spectrum. This was accounted for by applying a second filter (<0.06) to the absolute differences in reflectance between the red and blue bands. After applying the cloud mask to all cloud fields, we defined cloud objects by setting the pixel connectivity to four, i.e., pixels belong to the same object if their edges touch, but not if their corners touch. Clouds' morphological properties were calculated, including CSD, CF (CF_{calc}), the number of clouds in the field (N), and the distance of each cloud centroid from its nearest neighbor (NN) (see Fig. 3).

III. Results

A. Visual Classification of Cloud Fields

To characterize and examine green Cu fields over the world's continents, first, we had to distinguish the relevant fields from other cloud field types. Since the human eye is exceptional at detecting patterns, for this stage, we used visual classification. The three ROIs that often exhibit organized shallow Cu fields (as described in Section II-A) in the warm (dry) season (JJA) were chosen and investigated. Each ROI was divided into 1° × 1° cloud fields, which were then categorized into four different classes: 1) sparse (no clouds to a few shallow Cu); 2) organized shallow Cu (green Cu); 3) transition from shallow to deep convection (deeper clouds that appear as "puffy" organized shallow Cu and/or clustered organized shallow Cu, hereafter transition); and 4) deep convective (big clouds that cover most or even all of the cloud field, hereafter deep). We note that over the selected ROIs, other classes of clouds, such as shallow stratiform or cirrus, were not common. Classic examples for the four classes of cloud fields are shown in Fig. 2. Cloud fields that were not clearly associated with one of the four classes for reasons such as cirrus contamination, fires, and highly nonuniform fields, were excluded from the analysis.

The visual classification was performed for the period of July–August 2008 for the three ROIs. The classification resulted in a data set containing a total of 12 146 cloud fields, of which 2762 were classified as sparse, 2142 as green Cu, 2446 as transition, and 4796 as deep convective. Focusing on the green Cu class, Fig. 3 shows some key organization parameters–CSD, CF_{calc}, N, and NN, as calculated from the high-resolution images (see Fig. 3(a)–(d), respectively). As suspected by observing Fig. 1, Fig. 3 reveals that indeed, green Cu fields exhibit similar values in all of the inspected regions. When examining the CSD [see Fig. 3(a)], all of the curves showed almost identical behavior, with a peak at

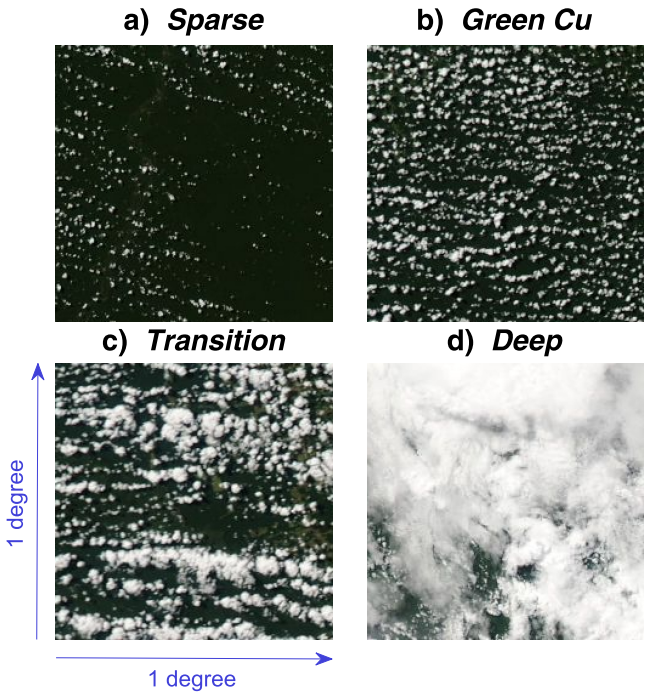

Fig. 2. 1° × 1° RGB images of the four different classes into which the cloud fields were visually classified. (a) Sparse. (b) Organized shallow cumulus (green Cu). (c) Transition from shallow to deep convection (*transition*). (d) Deep convection (deep).

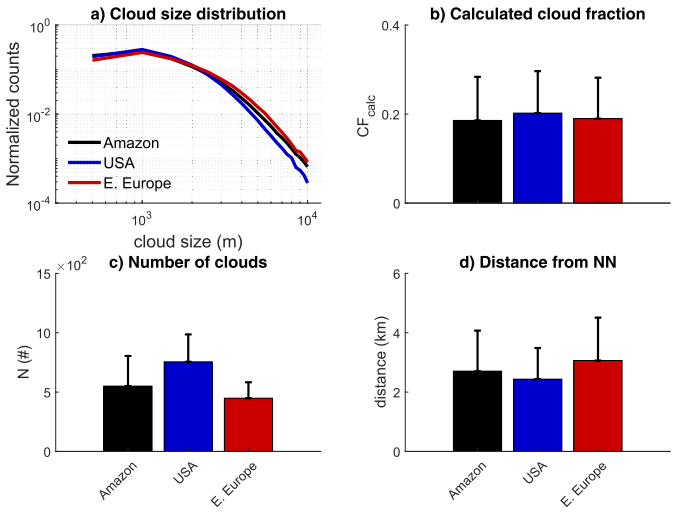

Fig. 3. Cloud field morphological parameters for the different ROIs (Amazon, black; USA, blue; Eastern [E.] Europe, red) as calculated from the high-resolution images. (a) CSD. (b) Calculated CF (CF_{calc}). (c) Number of clouds in a field (N). (d) Distance from the NN. Errors bars are STDs.

the cloud size of 1 km, in agreement with previous studies [11], [14]. We note that the CSD most likely underestimates the counts of the small clouds ($\leqslant$500 m) due to restrictions resulting from the image resolution. CF_{calc} was practically the same for all ROIs [ranging between 0.186 and 0.202, Fig. 3(b)], whereas N varied between ~450 deg^{-2} in Eastern Europe to ~550 deg^{-2} in the Amazon, and ~755 deg^{-2} in the USA [see Fig. 3(c)]. The more numerous clouds in the USA ROI are also evident in the CSD, which shows more of the smaller clouds and less of the bigger ones. In terms of mean NN, again, the values presented by the three ROIs converge to ~2.5 km. The parameters examined in Fig. 3 suggest similar organization patterns shared by the cloud fields in the different ROIs. However, they do not give direct evidence of the level or type of organization. We further inspected the organization exhibited by the cloud fields by calculating the NN cumulative density functions (NNCDFs) of the observed cloud fields and plotting them against the Poisson NNCDF, which represents a randomly distributed cloud field (with NNCDF given by the Weibull distribution; [51]). As evident from Fig. 4(a), the mean NNCDF curve for each ROI (each in a different color) deviates from randomness toward a more regular, grid-like pattern (i.e., all curves are below the diagonal, indicating that the number of clouds within a certain distance are less than that predicted by the theoretical random distribution). The organization index (I_{org}; [52]) for each ROI was then derived by integrating the area under each of the NNCDF graphs. While random convection yields $I_{org} = 0.5$, the mean values of the different ROIs are all smaller: $I_{org} = 0.45\pm0.09, 0.41\pm0.07, 0.44\pm0.08$ for the Amazon, USA, and Eastern Europe ROIs, respectively. Fig. 4(b) lays out the phase space spanned by I_{org} and the mean cloud object size, $S = (CF_{calc}/N) \times 10^4$ [53], to show the diversity of patterns exhibited by the different cloud fields. Although there is some natural variability between the different ROIs, as well as between different fields in the same region, most cases (>75%) fall in the lower left quadrant, suggesting the predominance of small clouds with a regular organization. Some of the cloud fields are located in the upper left quadrant of the phase space, indicating small clouds which are more clustered. Integrating the organization parameters shown in Fig. 3, with the analysis from the upper panels of Fig. 4, gives in consistent grid-like organization of the cloud fields in the different ROIs. A regular organization can be regarded as a private case of a linear organization pattern (also known as cloud streets), which is the case for many of the examined cloud fields. An example of such a case (from the Amazon region) is shown in Fig. 4(c) and marked by a star on the phase space in Fig. 4(b). The clouds are aligned along a preferred angle, which can be found using a Radon-like analysis by rotating the cloud-field image and summing the cloudy pixels (equivalent to intensity) over the image's rows [see Fig. 4(d)]. While the signal is noisy, and there might be a few preferred angles that correspond to different spatial scales in the field, it is evident that there is a distinct angle for which the summation of cloudy pixels is maximal. For this case, the preferred angle ($\theta = 26°$) deviates by more than two standard deviation (STD) units from the mean [light gray shaded area in Fig. 4(d)]. The binary cloud mask image rotated at $\theta = 26°$ is shown in Fig. 4(e).

B. Global Identification of Green Cu Fields

Post-classification, each 1° × 1° cloud field was assigned to the matching Aqua MODIS L3 cloud products (resolution of 1° × 1°): CF, CTH, and the associated STDs (see Fig. 5). The minimal number of cloud properties enabling successfully distinguishing between the different classes was chosen from the many cloud products offered by MODIS L3. Specifically,

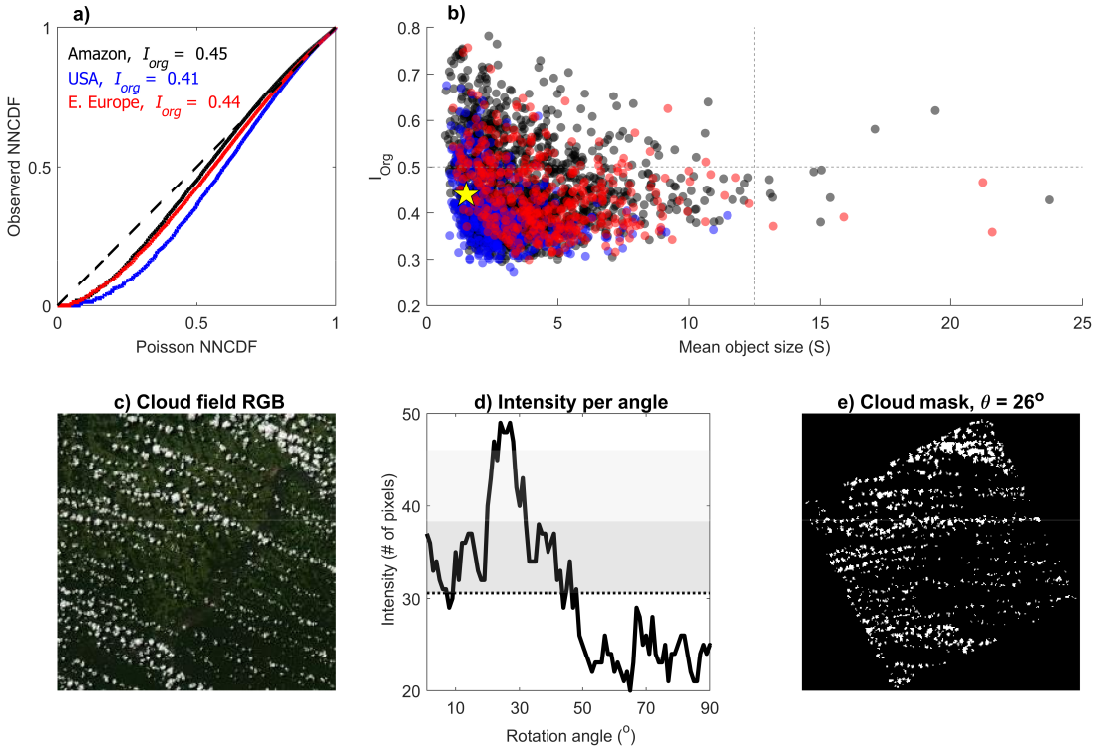

Fig. 4. (a) Observed NNCDF against Poisson NNCDF for the Amazon (black), USA (blue), and Eastern (E.) Europe (red) ROIs. The diagonal dashed line represents a perfectly randomly distributed cloud field, while deviations above (below) the diagonal indicate a tendency toward clustering (regularity). The mean organization index (I_{org} [52]) of each ROI is given in the top-left corner. (b) I_{org} against mean object size (S [53]). Different ROIs are represented by the colors specified in (a). Star marks specific case study that is examined in the lower panels. (c) True-color (RGB) image from the Amazon region that exhibits linear patterns. (d) Intensity (maximum number of cloudy pixels summed over the rows for different rotation angles). Black dotted line is the mean values; gray shaded area marks one unit of standard divination. (e) Binary image of the field's cloud mask rotated to the angle of the maximal sum of cloudy pixels ($\theta = 26°$).

CF and its STD were chosen because CF (sometimes referred to as cloud cover) is among the most basic, but also one of the most important properties of a cloud field. CTH and its STD were selected to ensure that we are indeed tackling warm clouds. Other cloud properties were examined as well (e.g., cloud top pressure, cloud top temperature, liquid water path, and cloud optical thickness) and were found to behave in a fashion that was consistent with the chosen parameters. Thus, these cloud properties were excluded from this analysis to avoid redundancy. As shown in Fig. 5, the three regions exhibit similar cloud field characteristics, confirming that the cloud fields identified for the different ROIs are also consistent in terms of cloud properties. As expected, L3 cloud properties (CF and CTH) increase as a function of the cloud field type (going from sparse to deep). The STDs of CF and CTH are standard MODIS L3 products that are derived from the higher resolution level-2 data (resolution of 1 km) and therefore can be used as a measure of the cloud's organization in the field. A low STD value indicates that the cloud field is uniform, for example, in the case of no clouds (such as some of the sparse cloud fields) or a large cloud that covers the whole field (such as some of the deep cloud fields). On the other hand, a high STD suggests that the cloud field is nonuniform. This can happen when the cloud field contains clouds of many different sizes (transition) or for a large cloud that covers a big portion of the field, but not all of it (as in some of the deep cloud field

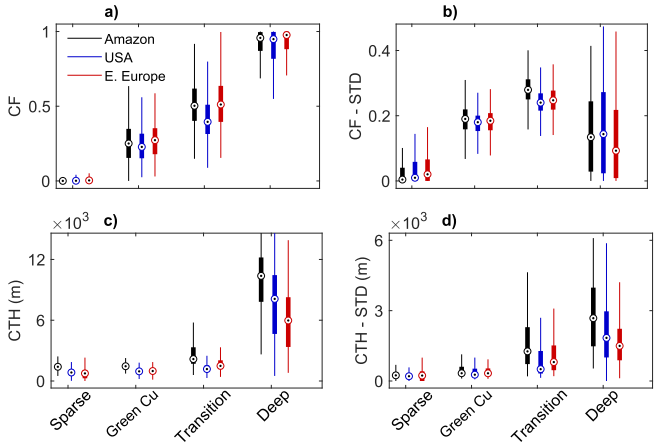

Fig. 5. Boxplot of MODIS L3 cloud properties assigned to the different classes of the visually classified cloud fields: sparse, green Cu, transition (from shallow to deep convection), and deep convection (deep). (a) CF and (c) CTH and (b) and (d) corresponding STDs, respectively. The Amazon, USA, and Eastern (E.) Europe ROIs are represented in black, blue, and red, respectively.

cases). For the case of green Cu, we expect a low-to-moderate STD for CF and CTH, as shown in Fig. 5(b) and (d).

Next, the MODIS L3 cloud properties (shown in Fig. 5) were used to detect green Cu fields on a global data set covering ten years (2003–2012). We applied the 10th and 90th

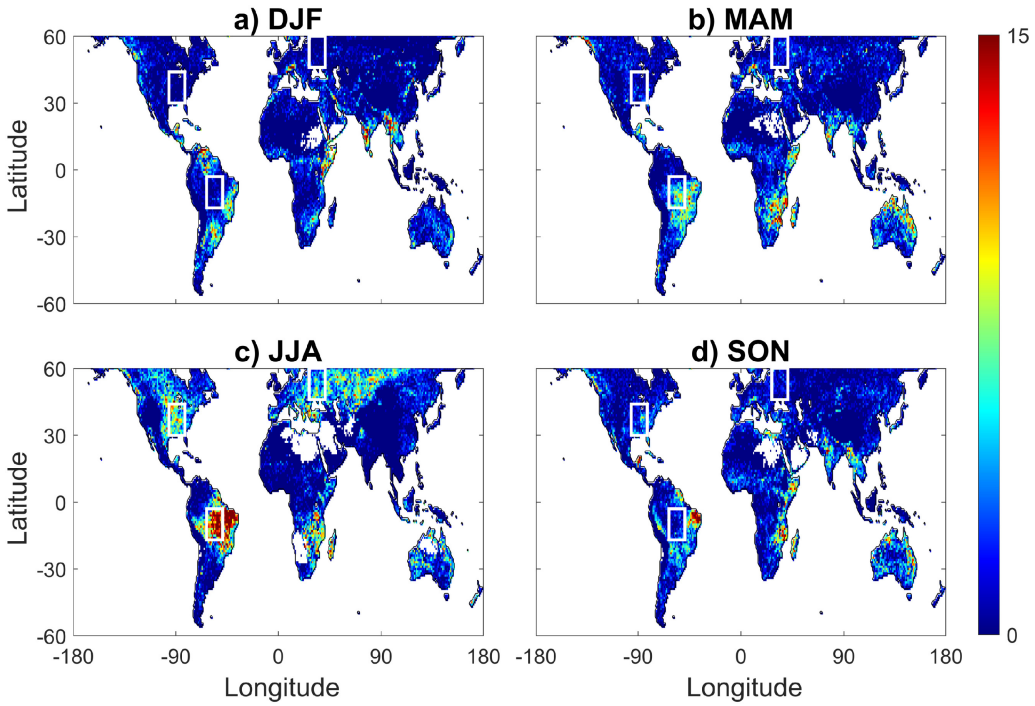

Fig. 6. Probability (%) of observing a green Cu field over land ($60°N - 60°S$) during (a) December–January–February (DJF), (b) March–April–May (MAM), (c) JJA, and (d) September–October–November (SON) for the years 2003–2012. White boxes represent the three ROIs. Note that the ROIs cover an area of $14° \times 14°$ [see Fig. 1(d)] but appear rectangular here due to vertical exaggeration. White areas are either oceans or pixels with not enough data due to failure of the MODIS L3 retrieval.

TABLE I

MEAN 10TH AND 90TH PERCENTILE VALUES USED AS LOWER AND UPPER THRESHOLDS TO IDENTIFY GREEN CU FIELDS OVER TEN YEARS (2003–2012) OF THE MODIS L3 DATA SET

Cloud Property	10 Percentile	90 Percentile
CF	0.093	0.446
CF-STD	0.125	0.242
CTH (m)	534.2	2088.0
CTH-STD (m)	170.0	1591.4

percentiles of CF, CTH, and their STDs (as presented in Table I) as the lower and upper thresholds to automatically identify green Cu fields and calculate their probability of occurrence.

Fig. 6 shows the global (60°N–60°S) spread of the occurrence probability of green Cu fields throughout the different seasons (along ten years). The highest probabilities for green Cu fields can be found mostly during JJA [see Fig. 6(c)] around the three ROIs but also in south-east Africa and Australia. The region where green Cu are most abundant is the Amazon basin, with values of up to ∼31% in JJA. Green Cu fields peak during JJA (NH summer; dry season in the Amazon) due to the stable meteorological conditions that support shallow convection over deeper clouds [20]. Green Cu are still evident in other seasons and other regions but to a lesser extent. The shift from one class of cloud field to another is not abrupt, but more of a smooth transition. For this reason, approaching the lower and upper limits of the distribution of the cloud properties used to identify green Cu (CF, CTH, and their STDs, see Fig. 5), there may be some overlap between the different classes. To minimize false detection of other cloud field classes as green Cu (i.e., false-positive errors), we applied a conservative approach that missed some of the green Cu cases (false-negative errors). We used restricted thresholds to identify green Cu (see narrow ranges in Table I). Other sources for false-negative errors stem from the coarse resolution and from MODIS retrieval errors and biases as, e.g., suggested by [54] and also from the presence of cirrus clouds that exhibit extremely high CTH values, even though they might be completely transparent in the high-resolution RGB images (i.e., cirrus contamination). We, therefore, note that the maps shown in Fig. 6 constitute a lower bound estimate for green Cu probabilities. Moreover, detailed examination of the high-resolution images of the cloud fields classified as sparse and transition showed that these fields are essentially derivatives of green Cu fields. For example, a sparse field can be thought of as a forming or dissipating green Cu field, and a transition field might simply be the deepening and/or clustering of a green Cu field. For this study, since we are interested in the unique organization pattern of green Cu fields, we restricted the classification to identify only the classical green Cu fields. Nonetheless, for other purposes (e.g., climatological analysis), the selected thresholds can be relaxed to better represent the probability of occurrence of green Cu. When relaxing the thresholds and applying, e.g., the 1st and 99th percentiles of CF, CTH, and their STDs, thus allowing for more false-positive, but less false-negative errors, the probabilities increase in all regions, and reach ∼69% in the Amazon in JJA (not shown).

When examining the JJA green Cu probability map [see Fig. 6(c)] against the ESA CCI-LC project [47], it is evident that these cloud fields are indeed associated with

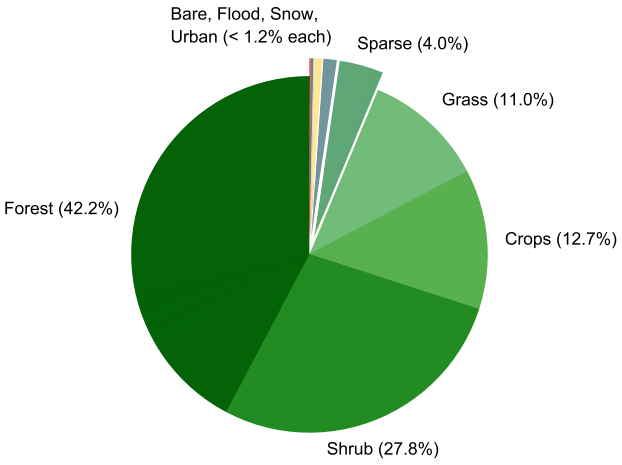

Fig. 7. Pie chart showing the frequency of occurrence of green Cu with the probability of >5% over different land cover types.

vegetated areas, therefore supporting the initial observation and affirming their label as green Cu; 42.2% of green Cu (with the probability of >5%) occur above forests, 27.8% above shrublands, 12.7% above croplands, 11.0% above grasslands, and 4.0% above sparsely vegetated areas (see Fig. 7). Green Cu fields are not likely to occur above bare, flood, snow, or urban areas (<1.2% each).

IV. Summary and Conclusion

We show that a significant portion of the shallow continental convective cloud fields shares common properties, although they are distributed globally and form under a variety of climatic conditions [see Fig. 1(a)–(c)]. We used different remote-sensing data sets to explore this novel observation of emerging universality on a global scale. We examined three ROIs located over the tropics, and mid and high latitudes (see Fig. 1(d); Amazon basin, central USA, and Eastern Europe, respectively) and visually classified two months of high-resolution Aqua MODIS RGB images into four different classes of cloud fields: sparse, green Cu, transition, and deep (see Fig. 2). Analysis of the visually classified green Cu fields showed similar organizational patterns, as expressed by properties such as CSD, CF_{calc}, N, and NN (see Fig. 3). Moreover, by examining the NNCDF of those cloud fields and comparing it to a theoretical random distribution (Poisson NNCDF), we found that the cloud fields deviate from randomness and exhibit a similar regular organizational pattern [see Fig. 4(a)], with $I_{org} < 0.5$ in all ROIs. We showed that over 75% of the green Cu fields are located in the lower left quadrant of the phase space spanned by the I_{org} and the mean object size (S) [see Fig. 4(b)], indicating small shallow clouds that are organized in a grid-like manner. A regular field is a private case of a linearly organized shallow cloud field (cloud streets), which is a prevalent pattern in many of the green Cu cases. We used an example of such a field to show that the clouds exhibit a preferred alignment direction [see Fig. 4(c)–(e)].

Next, by assigning each classified cloud field class with the matching coarser resolution (1° × 1°) MODIS L3 data, we showed that green Cu share similar cloud properties on this scale as well (CF, CTH, and their STDs, see Fig. 5). This allowed us to tune specific thresholds (see Table I) and use the coarser resolution MODIS L3 data set to globally detect green Cu fields for a period of ten years. By exploring the global (60° N–60° S) probability maps (see Fig. 6), we show that green Cu are most abundant in the Amazon during the dry season (JJA), with values reaching as high as ∼31%. Furthermore, we suggest that this value is a lower limit for green Cu occurrence since we used coarse resolution cloud properties and conservative thresholds (to minimize false-positive errors). In fact, green Cu are probably more ubiquitous both in space and time. When relaxing the thresholds and capturing more of the green Cu fields (but also more of the sparse and transition fields), probability values can reach ∼69% in the Amazon (depending on the specific thresholds used). In future work, we plan to zoom-in to specific areas and examine green Cu in additional regions, such as Africa, Australia, and China.

Finally, by examining the land cover above which we found a high probability of green Cu occurrence, it could be concluded that these clouds preferably form over vegetated areas. Specifically, it seems that they form over forests, shrublands, croplands, and grasslands (see Fig. 7). In forests and other vegetated regions, the soil and vegetation are moist enough to provide a source of water for the atmosphere through evapotranspiration, consisting mainly of plant transpiration and bare soil evaporation [55]. The land cover properties (e.g., vegetation cover, soil moisture, surface roughness, and soil type) mediate the surface fluxes, and therefore the exchange of energy and moisture, and the partitioning between sensible and latent heat (i.e., the Bowen ratio) [56], [57]; this affects cloud formation and properties [29], [58]–[61] and creates conditions that favor the formation of green Cu.

Here, we show that a subset of the continental warm Cu fields, defined as green Cu because of their strong association to vegetated areas, shows robust universal characteristics. The links of the reported properties to dynamic and microphysical processes should be further explored in future work, but such information on formation conditions and cloud fields properties can serve to better parameterize subgrid cloud fields in GCMs. Therefore, future GCMs will be able to consider not only bulk properties of clouds but also subgrid morphological information, such as clouds' organization patterns. This will advance and improve cloud representations in GCMs in terms of radiative and thermodynamic effects.

Acknowledgment

All data used in this study are publicly available and can be found at https://ladsweb.modaps.eosdis.nasa.gov/ (MODIS L3 data), https://worldview.earthdata.nasa.gov/ (MODIS GeoTiff images), and https://www.esa-landcover-cci.org/ (ESA-CCI land cover data). All other data used have been cited, with details provided in the references.

References

[1] K. E. Trenberth, J. T. Fasullo, and J. Kiehl, "Earth's global energy budget," *Bull. Amer. Meteorol. Soc.*, vol. 90, no. 3, pp. 311–323, Mar. 2009.

[2] P. Forster *et al.*, *Climate Change 2007-The Physical Science Basis: Working Group I Contribution to the Fourth Assessment Report of the IPCC*, D. Qin, M. Manning, Z. Chen, M. Marquis, K. B. Averyt, M. Tignor, and H. L. Miller, Eds. Cambridge, U.K.: Cambridge Univ. Press, 2007, pp. 129–234, ch. 2.

[3] O. Boucher *et al.*, "Clouds and aerosols," in *Climate Change 2013: The Physical Science Basis. Contribution of Working Group I to the Fifth Assessment Report of the Intergovernmental Panel on Climate Change*. Cambridge, U.K.: Cambridge Univ. Press, 2013, pp. 571–657.

[4] T. Schneider *et al.*, "Climate goals and computing the future of clouds," *Nature Climate Change*, vol. 7, no. 1, pp. 3–5, Jan. 2017.

[5] S. Bony, "Marine boundary layer clouds at the heart of tropical cloud feedback uncertainties in climate models," *Geophys. Res. Lett.*, vol. 32, no. 20, 2005, Art. no. L20806.

[6] G. Dagan, I. Koren, O. Altaratz, and G. Feingold, "Feedback mechanisms of shallow convective clouds in a warmer climate as demonstrated by changes in buoyancy," *Environ. Res. Lett.*, vol. 13, no. 5, May 2018, Art. no. 054033.

[7] S. Platnick *et al.*, "The MODIS cloud products: Algorithms and examples from Terra," *IEEE Trans. Geosci. Remote Sens.*, vol. 41, no. 2, pp. 459–473, Feb. 2003.

[8] D. D. Turner *et al.*, "Thin liquid water clouds: Their importance and our challenge," *Bull. Amer. Meteorol. Soc.*, vol. 88, no. 2, pp. 177–190, Feb. 2007.

[9] L. K. Berg and E. I. Kassianov, "Temporal variability of fair-weather cumulus statistics at the ACRF SGP site," *J. Climate*, vol. 21, no. 13, pp. 3344–3358, Jul. 2008.

[10] L. K. Berg, E. I. Kassianov, C. N. Long, and D. L. Mills, "Surface summertime radiative forcing by shallow cumuli at the atmospheric radiation measurement southern great plains site," *J. Geophys. Res.*, vol. 116, no. D1, 2011, Art. no. D01202.

[11] Y. Zhang and S. A. Klein, "Factors controlling the vertical extent of fair-weather shallow cumulus clouds over land: Investigation of diurnal-cycle observations collected at the ARM southern great plains site," *J. Atmos. Sci.*, vol. 70, no. 4, pp. 1297–1315, Apr. 2013.

[12] G. Lenderink *et al.*, "The diurnal cycle of shallow cumulus clouds over land: A single-column model intercomparison study," *Quart. J. Roy. Meteorol. Soc.*, vol. 130, no. 604, pp. 3339–3364, Oct. 2004.

[13] A. R. Brown *et al.*, "Large-eddy simulation of the diurnal cycle of shallow cumulus convection over land," *Quart. J. Roy. Meteorol. Soc.*, vol. 128, no. 582, pp. 1075–1093, Apr. 2002.

[14] K. Lamer and P. Kollias, "Observations of fair-weather cumuli over land: Dynamical factors controlling cloud size and cover," *Geophys. Res. Lett.*, vol. 42, no. 20, pp. 8693–8701, Oct. 2015.

[15] R. A. J. Neggers and A. P. Siebesma, "Constraining a system of interacting parameterizations through multiple-parameter evaluation: Tracing a compensating error between cloud vertical structure and cloud overlap," *J. Climate*, vol. 26, no. 17, pp. 6698–6715, Sep. 2013.

[16] J. Vial, S. Bony, J. Dufresne, and R. Roehrig, "Coupling between lower-tropospheric convective mixing and low-level clouds: Physical mechanisms and dependence on convection scheme," *J. Adv. Model. Earth Syst.*, vol. 8, no. 4, pp. 1892–1911, Dec. 2016.

[17] A. Dai and K. E. Trenberth, "The diurnal cycle and its depiction in the community climate system model," *J. Climate*, vol. 17, no. 5, pp. 930–951, Mar. 2004.

[18] M. Ahlgrimm and R. Forbes, "The impact of low clouds on surface shortwave radiation in the ECMWF model," *Monthly Weather Rev.*, vol. 140, no. 11, pp. 3783–3794, Nov. 2012.

[19] J. Pergaud, V. Masson, S. Malardel, and F. Couvreux, "A parameterization of dry thermals and shallow cumuli for mesoscale numerical weather prediction," *Boundary-Layer Meteorol.*, vol. 132, no. 1, p. 83, 2009.

[20] N. P. Wilde, R. B. Stull, and E. W. Eloranta, "The LCL zone and cumulus onset," *J. Climate Appl. Meteorol.*, vol. 24, no. 7, pp. 640–657, Jul. 1985.

[21] P. Zhu, "Large eddy simulations of continental shallow cumulus convection," *J. Geophys. Res.*, vol. 108, no. D15, p. 4453, 2003.

[22] Y. Zhang *et al.*, "Large-eddy simulation of shallow cumulus over land: A composite case based on ARM long-term observations at its Southern Great Plains site," *J. Atmos. Sci.*, vol. 74, no. 10, pp. 3229–3251, Oct. 2017.

[23] Y. Zhang and S. A. Klein, "Mechanisms affecting the transition from shallow to deep convection over land: Inferences from observations of the diurnal cycle collected at the ARM Southern Great Plains site," *J. Atmos. Sci.*, vol. 67, no. 9, pp. 2943–2959, Sep. 2010.

[24] Y. Zhuang, R. Fu, J. A. Marengo, and H. Wang, "Seasonal variation of shallow-to-deep convection transition and its link to the environmental conditions over the Central Amazon," *J. Geophys. Res., Atmos.*, vol. 122, no. 5, pp. 2649–2666, Mar. 2017.

[25] E. Kassianov, E. A. Riley, J. M. Kleiss, L. D. Riihimaki, and L. K. Berg, "Macrophysical properties of continental shallow cumuli: Diurnal evolution," in *Proc. 24th Int. Soc. Opt. Photon., Remote Sens. Clouds Atmos.*, vol. 11152, 2019, Art. no. 111520A.

[26] K.-S. Sunny Lim *et al.*, "Long-term retrievals of cloud type and fair-weather shallow cumulus events at the ARM SGP site," *J. Atmos. Ocean. Technol.*, vol. 36, no. 10, pp. 2031–2043, Oct. 2019.

[27] E. Cutrim, D. W. Martin, and R. Rabin, "Enhancement of cumulus clouds over deforested lands in Amazonia," *Bull. Amer. Meteorol. Soc.*, vol. 76, no. 10, pp. 1801–1805, Oct. 1995.

[28] F. J. F. Chagnon, "Climatic shift in patterns of shallow clouds over the Amazon," *Geophys. Res. Lett.*, vol. 31, no. 24, 2004, Art. no. L24212.

[29] R. H. Heiblum, I. Koren, and G. Feingold, "On the link between amazonian forest properties and shallow cumulus cloud fields," *Atmos. Chem. Phys.*, vol. 14, no. 12, pp. 6063–6074, Jun. 2014.

[30] V. G. Plank, "The size distribution of cumulus clouds in representative florida populations," *J. Appl. Meteorol.*, vol. 8, no. 1, pp. 46–67, Feb. 1969.

[31] B. A. Wielicki and R. M. Welch, "Cumulus cloud properties derived using landsat satellite data," *J. Climate Appl. Meteorol.*, vol. 25, no. 3, pp. 261–276, Mar. 1986.

[32] D. E. Lane, K. Goris, and R. C. J. Somerville, "Radiative transfer through broken clouds: Observations and model validation," *J. Climate*, vol. 15, no. 20, pp. 2921–2933, Oct. 2002.

[33] T. C. Benner and J. A. Curry, "Characteristics of small tropical cumulus clouds and their impact on the environment," *J. Geophys. Res., Atmos.*, vol. 103, no. D22, pp. 28753–28767, Nov. 1998.

[34] R. A. J. Neggers, H. J. J. Jonker, and A. P. Siebesma, "Size statistics of cumulus cloud populations in large-eddy simulations," *J. Atmos. Sci.*, vol. 60, no. 8, pp. 1060–1074, Apr. 2003.

[35] H. Jiang *et al.*, "Statistical comparison of properties of simulated and observed cumulus clouds in the vicinity of Houston during the Gulf of Mexico atmospheric composition and climate study (GoMACCS)," *J. Geophys. Res.*, vol. 113, no. D13, 2008, Art. no. D13205.

[36] T. Heus and A. Seifert, "Automated tracking of shallow cumulus clouds in large domain, long duration large eddy simulations," *Geosci. Model. Develop.*, vol. 6, no. 4, p. 1261, 2013.

[37] T. W. van Laar, V. Schemann, and R. A. J. Neggers, "Investigating the diurnal evolution of the cloud size distribution of continental cumulus convection using multiday LES," *J. Atmos. Sci.*, vol. 76, no. 3, pp. 729–747, Mar. 2019.

[38] W. P. Köppen, *Die klimate der erde: Grundriss der klimakunde*. Berlin, Germany: Walter de Gruyter, 1923.

[39] C. A. Nobre, L. F. Mattos, C. P. Dereczynski, T. A. Tarasova, and I. V. Trosnikov, "Overview of atmospheric conditions during the smoke, clouds, and radiation-Brazil (SCAR-B) field experiment," *J. Geophys. Res., Atmos.*, vol. 103, no. D24, pp. 31809–31820, Dec. 1998.

[40] E. K. M. Chang, S. Lee, and K. L. Swanson, "Storm track dynamics," *J. Climate*, vol. 15, no. 16, pp. 2163–2183, Aug. 2002.

[41] L. M. Whittaker and L. H. Horn, "Geographical and seasonal distribution of North American cyclogenesis, 1958–1977," *Monthly Weather Rev.*, vol. 109, no. 11, pp. 2312–2322, Nov. 1981.

[42] S. S. Parker, J. T. Hawes, S. J. Colucci, and B. P. Hayden, "Climatology of 500 mb cyclones and anticyclones, 1950–85," *Monthly Weather Rev.*, vol. 117, no. 3, pp. 558–571, Mar. 1989.

[43] P. Zhu and B. Albrecht, "A theoretical and observational analysis on the formation of fair-weather cumuli," *J. Atmos. Sci.*, vol. 59, no. 12, pp. 1983–2005, Jun. 2002.

[44] L. A. Remer *et al.*, "The MODIS aerosol algorithm, products, and validation," *J. Atmos. Sci.*, vol. 62, no. 4, pp. 947–973, 2005.

[45] R. C. Levy *et al.*, "The collection 6 MODIS aerosol products over land and ocean," *Atmos. Meas. Techn.*, vol. 6, no. 11, pp. 2989–3034, Nov. 2013. [Online]. Available: https://www.atmos-meas-tech.net/6/2989/2013/

[46] A. M. Sayer, N. C. Hsu, and C. Bettenhausen, "Implications of MODIS bow-tie distortion on aerosol optical depth retrievals, and techniques for mitigation," *Atmos. Meas. Techn.*, vol. 8, no. 12, pp. 5277–5288, Dec. 2015.

[47] G. Kirches *et al.*, *Land Cover CCI-Product User Guide-Version 2*, ESA Public document CCI-LC-PUG 2.4, 2014.

[48] G. J. Jedlovec, S. L. Haines, and F. J. LaFontaine, "Spatial and temporal varying thresholds for cloud detection in GOES imagery," *IEEE Trans. Geosci. Remote Sens.*, vol. 46, no. 6, pp. 1705–1717, Jun. 2008.
[49] X.-Y. Zhuge, X. Zou, and Y. Wang, "A fast cloud detection algorithm applicable to monitoring and nowcasting of daytime cloud systems," *IEEE Trans. Geosci. Remote Sens.*, vol. 55, no. 11, pp. 6111–6119, Nov. 2017.
[50] J. H. Jeppesen, R. H. Jacobsen, F. Inceoglu, and T. S. Toftegaard, "A cloud detection algorithm for satellite imagery based on deep learning," *Remote Sens. Environ.*, vol. 229, pp. 247–259, Aug. 2019.
[51] R. Weger, J. Lee, T. Zhu, and R. Welch, "Clustering, randomness and regularity in cloud fields: 1. theoretical considerations," *J. Geophys. Res., Atmos.*, vol. 97, no. D18, pp. 20519–20536, 1992.
[52] A. M. Tompkins and A. G. Semie, "Organization of tropical convection in low vertical wind shears: Role of updraft entrainment," *J. Adv. Model. Earth Syst.*, vol. 9, no. 2, pp. 1046–1068, Jun. 2017.
[53] S. Bony, H. Schulz, J. Vial, and B. Stevens, "Sugar, gravel, fish, and flowers: Dependence of mesoscale patterns of trade-wind clouds on environmental conditions," *Geophys. Res. Lett.*, vol. 47, no. 7, Apr. 2020.
[54] X. Zhuge, X. Zou, and Y. Wang, "Determining AHI cloud-top phase and intercomparisons with MODIS products over North Pacific," *IEEE Trans. Geosci. Remote Sens.*, early access, May 19, 2020, doi: 10.1109/TGRS.2020.2990955.
[55] S. I. Seneviratne, "Investigating soil moisture–climate interactions in a changing climate: A review," *Earth-Sci. Rev.*, vol. 99, no. 3, pp. 125–161, May 2010.
[56] G. B. Bonan, "Forests and climate change: Forcings, feedbacks, and the climate benefits of forests," *Science*, vol. 320, no. 5882, pp. 1444–1449, Jun. 2008.
[57] D. Sheil, "Forests, atmospheric water and an uncertain future: The new biology of the global water cycle," *Forest Ecosyst.*, vol. 5, no. 1, p. 19, Dec. 2018.
[58] F. Chen and R. Avissar, "Impact of land-surface moisture variability on local shallow convective cumulus and precipitation in large-scale models," *J. Appl. Meteorol.*, vol. 33, no. 12, pp. 1382–1401, Dec. 1994.
[59] R. M. Rabin and D. W. Martin, "Satellite observations of shallow cumulus coverage over the central united states: An exploration of land use impact on cloud cover," *J. Geophys. Res., Atmos.*, vol. 101, no. D3, pp. 7149–7155, Mar. 1996.
[60] D. V. Spracklen, S. R. Arnold, and C. Taylor, "Observations of increased tropical rainfall preceded by air passage over forests," *Nature*, vol. 489, no. 7415, p. 282, 2012.
[61] D. V. Spracklen, J. C. A. Baker, L. Garcia-Carreras, and J. H. Marsham, "The effects of tropical vegetation on rainfall," *Annu. Rev. Environ. Resour.*, vol. 43, no. 1, pp. 193–218, Oct. 2018.

Tom Dror received the B.Sc. degree in climate, atmospheric science and oceanography from the Hebrew University of Jerusalem, Jerusalem, Israel, in 2012, and the M.Sc. degree in atmospheric science from the Weizmann Institute of Science, Rehovot, Israel, in 2018, where she is pursuing the Ph.D. degree with the Earth and Planetary Sciences Department.

Her research interests include cloud physics and remote sensing of clouds, cloud field organization, aerosol–cloud interactions, and ocean–atmosphere interactions.

Ilan Koren received the Ph.D. degree in cloud physics from the Department of Geophysics and Planetary Sciences, Tel Aviv University, Tel Aviv, Israel, in 2002.

He then spent three years conducting postdoctoral research with the NASA's Goddard Space Flight Center's Climate and Radiation Branch before joining the Weizmann Institute of Science, Rehovot, Israel, in 2005. His research interests are in cloud and rain physics and ocean-atmosphere interactions. He explores theoretical aspects of complex systems and uses clouds and rain as a model to explore pattern formation and self-organizing systems.

Dr. Koren received the International Radiation Commission-Young Scientist Award in 2008 and the Krill Prize for Excellence in Scientific Research in 2009. He was a recipient of the two ERC Grants, in 2012 and 2019.

Orit Altaratz received the B.Sc. degree in geophysics and atmospheric sciences and the M.Sc. and Ph.D. degrees from Tel Aviv University, Tel Aviv, Israel, in 1995, 1997, and 2004, respectively.

She is an Associate Staff Scientist with the Department of Earth and Planetary Sciences, Weizmann Institute of Science, Rehovot, Israel. Her research interests include cloud physics, cloud-aerosol interactions, atmospheric electricity, and remote sensing of clouds.

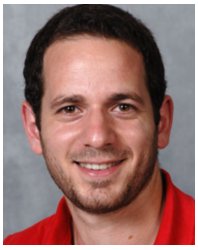

Reuven H. Heiblum received the B.Sc. degree in physics from Tel Aviv University, Tel Aviv, Israel, in 2008, and the M.Sc. and Ph.D. degrees in atmospheric sciences from the Weizmann Institute of Science, Rehovot, Israel, in 2012 and 2017, respectively.

Since 2017, he has been a Consultant with the Earth and Planetary Sciences Department, Weizmann Institute and has been with Mobile Physics Ltd., Kfar Saba, Israel, developing new technology for environmental measurements since 2019. His research interests include cloud field organization and precipitation, remote sensing of aerosols, and dynamic meteorology in the Mediterranean region.